

Ion production rate in a boreal forest based on ion, particle and radiation measurements

L. Laakso¹, T. Petäjä¹, K. E. J. Lehtinen¹, M. Kulmala¹, J. Paatero², U. Hörrak³,
H. Tammet³, and J. Joutsensaari⁴

¹Department of Physical Sciences, P.O. Box 64, FIN-00014 University of Helsinki, Finland

²Finnish Meteorological Institute, Air Quality Research, Sahaajankatu 20E, FIN-00880
Helsinki, Finland

³Institute of Environmental Physics, University of Tartu, 18 Ülikooli Street, Tartu, 50090,
Estonia

⁴Department of Applied Physics, University of Kuopio, P.O. Box 1627, FIN-70211 Kuopio,
Finland

Received: 23 April 2004 – Accepted: 18 May 2004 – Published: 20 July 2004

Correspondence to: L. Laakso (lauri.laakso@iki.fi)

Ion production rate

L. Laakso et al.

[Title Page](#)

[Abstract](#)

[Introduction](#)

[Conclusions](#)

[References](#)

[Tables](#)

[Figures](#)

[◀](#)

[▶](#)

[◀](#)

[▶](#)

[Back](#)

[Close](#)

[Full Screen / Esc](#)

[Print Version](#)

[Interactive Discussion](#)

© EGU 2004

In this study the ion production rates in a boreal forest are studied based on two different methods: 1) cluster ion and particle concentration measurements, 2) external radiation and radon concentration measurements. Both methods produce reasonable estimates for ion production rates. The average ion production rate calculated from aerosol particle size distribution and air ion mobility distribution measurements was 5 $2.6 \text{ cm}^{-3} \text{ s}^{-1}$ and based on external radiation and radon measurements $4.5 \text{ cm}^{-3} \text{ s}^{-1}$. The first method based on ion and particle measurements gave lower values for the ion production rates especially during the day. A possible reason for this is that particle 10 measurements started only from 3 nm, so the sink of small ions during the nucleation events was underestimated. Another reason is that the possible fogs, which caused an extra sink of small ions are not taken into account in the calculations. It may also be possible that the hygroscopic growth factors of aerosol particles were underestimated. A fourth possible reason for the discrepancy is the nucleation mechanism itself. If the 15 ions were somehow present in the nucleation process, there could have been an additional ion sink during the nucleation days. On the other hand, not all the radiation energy is converted to ions and the possible effect of alpha recoil is also omitted.

1. Introduction

Nucleation followed by particle growth has recently been observed at various locations 20 and by several research groups (see overview by [Kulmala et al., 2004](#), and references therein). Although these bursts of new particles have been frequently observed, the mechanisms of particle formation still remain unclear. Several nucleation mechanisms have been proposed, including classical binary homogeneous nucleation, ternary nucleation ([Kulmala et al., 2000a](#)), ion-induced nucleation and ion-mediated nucleation 25 ([Yu and Turco, 2000](#)). Recent results indicate the possibility of barrierless nucleation ([Laakso et al., 2004](#)). None of the mechanisms have been confirmed or rejected yet

Ion production rate

L. Laakso et al.

[Title Page](#)

[Abstract](#)

[Introduction](#)

[Conclusions](#)

[References](#)

[Tables](#)

[Figures](#)

[◀](#)

[▶](#)

[◀](#)

[▶](#)

[Back](#)

[Close](#)

[Full Screen / Esc](#)

[Print Version](#)

[Interactive Discussion](#)

© EGU 2004

and it may be possible, that several of these mechanisms are simultaneously active in the atmosphere.

In the case of ion-induced nucleation, the nucleation rate is always limited by the ion production rate. Even if condensation is enhanced by electric interactions (Yu and Turco, 2000), still the maximum nucleation rate is equal to the ion production rate. This is one of the reasons why the ion production rate is such a key quantity in atmospheric physics. The measurements of the ionization rate can be divided into two group: direct measurements by means of ionization chambers and indirect measurements based on calculations according to the balance equation of small air ions. For comparison, the data should be complemented by the method of measurements, measuring height and time (summer/winter).

Overviews of the earlier measurements (mainly before 1950) of the ionization rate can be found in (Israel, 1970, 1973; Chalmers, 1967). The average ionization rate at 1 m height from the ground of approximately $10 \text{ ion pairs cm}^{-3} \text{s}^{-1}$ is considered as a standard for continental areas. Three main ionizing agencies (factors) have the following contributions: the ionization caused by radioactive substances in the ground is about $4.6 \text{ ion pairs cm}^{-3} \text{s}^{-1}$ and in the air (radon, radioactive aerosol) $4 \text{ ion pairs cm}^{-3} \text{s}^{-1}$, and by cosmic radiation from 1.5 to $1.8 \text{ ion pairs cm}^{-3} \text{s}^{-1}$ (Israel, 1970, 1973; Chalmers, 1967). Considering different locations, the ionization rate could exhibit considerable variation depending on the content of radioactive substances in the ground, on the soil properties, on the water content of the snow cover, and due to local orography. The measurements below 1 m strongly depend (many times) on the ionization profile. The ionization rate decreases with altitude near the ground up to about 1–2 km, and increases again towards higher altitudes up to about 15 km (maximum about $50 \text{ ion pairs cm}^{-3} \text{s}^{-1}$) (Hoppel et al., 1986; Mohnen, 1977; Rosen et al., 1985). In continental areas, the ionization rate is an indicator of environmental radioactivity; its variation is weakly influenced by cosmic rays. The temporal variation of the ionization rate (annual and diurnal variation) is mostly due to the variation in radon and thoron concentration. The ionization rate can be used as an indicator of stability of boundary

Ion production rate

L. Laakso et al.

[Title Page](#)

[Abstract](#)

[Introduction](#)

[Conclusions](#)

[References](#)

[Tables](#)

[Figures](#)

[◀](#)

[▶](#)

[◀](#)

[▶](#)

[Back](#)

[Close](#)

[Full Screen / Esc](#)

[Print Version](#)

[Interactive Discussion](#)

© EGU 2004

layer just like the concentration of radon (Porstendörfer, 1994; Kataoka et al., 1998). Galactic cosmic rays (GCR) are the primary ionizing source above the oceans. The intensity of the cosmic rays in the atmosphere is modulated by the 11-year solar cycle. This modulation increases as a function of height (Larsen, 1993). A comprehensive list of the measurements of ionization rate in marine environment can be found in Hensen and van der Hage (1994).

Reports of some more recent measurements of ionization rates can be found in (Dhanorkar and Kamra, 1994; Wilkening, 1985; Mochizuki et al., 1977; Hensen and van der Hage, 1994). Dhanorkar and Kamra (1994) have used a set of integral ion counters to measure small ion concentration and aerosol ion mobility distribution at a height of about 1 m above the ground at Pune, India. The ionization rate was calculated based on the balance equation. The results presented for the two days displayed the diurnal variation in the ionization rate with the minimum at noon $2.75 \text{ cm}^{-3} \text{ s}^{-1}$ and very high maximum in the early morning $117 \text{ cm}^{-3} \text{ s}^{-1}$. Wilkening (1985) measured small ion and radon concentrations at two locations and in Carlsbad Caverns in southwestern United States. The ion pair production rates have been estimated from a knowledge of the radon (^{220}Rn , ^{222}Rn) concentrations, and their daughters under equilibrium conditions in outdoor air, and from published values of cosmic ray fluxes. The estimated ion production rates for the Langmuir Laboratory for Atmospheric Research (3240 m msl) and for Rio Grande Valley at Socorro (1410 m) were 10 and $15 \text{ cm}^{-3} \text{ s}^{-1}$, respectively. The estimate for Carlsbad Caverns (230 m underground, surface elevation 1340 m) was $2300 \text{ cm}^{-3} \text{ s}^{-1}$. Mochizuki et al. (1977) developed and built an ionization chamber for continuous monitoring of the ion formation rate in the atmosphere. Results of one day measurements at two different levels (0.2 m and 1 m) have been presented. The diurnal variation of the ionization rate at 1 m height has the minimum at noon of about $6 \text{ cm}^{-3} \text{ s}^{-1}$ and the maximum during nighttime of about $13 \text{ cm}^{-3} \text{ s}^{-1}$. The ionization rate at the height of 0.2 m displayed the same regularities, but was about two times higher (minimum $10 \text{ cm}^{-3} \text{ s}^{-1}$ and maximum $22 \text{ cm}^{-3} \text{ s}^{-1}$). This can be attributed to the steep radon concentration gradient in the air close to the ground (Liu et al., 1984).

Ion production rate

L. Laakso et al.

[Title Page](#)

[Abstract](#)

[Introduction](#)

[Conclusions](#)

[References](#)

[Tables](#)

[Figures](#)

[◀](#)

[▶](#)

[◀](#)

[▶](#)

[Back](#)

[Close](#)

[Full Screen / Esc](#)

[Print Version](#)

[Interactive Discussion](#)

© EGU 2004

Measurements in a marine environment depicted a variation in the ionization rate from 1.5 to $2.9 \text{ cm}^{-3} \text{ s}^{-1}$ considering different geomagnetic latitudes (Hensen and van der Hague, 1994).

The atmospheric-electric fog effect (the dependence of small ion concentration or air conductivity on the intensity of fog) is described in Hoppel et al. (1986); Dolazalek (1963).

Since ion production rate is such a crucial factor when investigating the charging state of aerosols and the possibility of ion-induced nucleation, it is investigated in further detail, in this case in a Finnish boreal forest. Two independent experimental methods for obtaining the ion production rate are compared. The first method is based on the measurements of radon and external radiation and the second method on the balance equation of small cluster ions. The experiments were carried out during the QUEST 2-measurement campaign in spring 2003. As a result of the study, an estimate of ion production rate in SMEAR II-measurement station ($61^{\circ}51' \text{ N}$, $24^{\circ}17' \text{ E}$, 180 m above sea level)(Vesala et al., 1998; Kulmala et al., 2001) in Hyytälä in Southern central Finland is given.

2. Experimental setup and theory

In this study several different instruments were utilized. The mobility distribution of the ions was measured with a Balanced Scanning Mobility Analyzer (BSMA), of the particles with two differential mobility particle sizers (DMPS) and an aerodynamical particle sizer (APS). The ionizing radiation was measured by glass-fibre filters and scintillation gamma spectrometer. All instruments are explained in more detail in the next sections.

Ion production rate

L. Laakso et al.

[Title Page](#)

[Abstract](#)

[Introduction](#)

[Conclusions](#)

[References](#)

[Tables](#)

[Figures](#)

[◀](#)

[▶](#)

[◀](#)

[▶](#)

[Back](#)

[Close](#)

[Full Screen / Esc](#)

[Print Version](#)

[Interactive Discussion](#)

© EGU 2004

2.1. BSMA

The Balanced Scanning Mobility Analyzer manufactured by Airel Ltd., Estonia, consists of two plain aspiration-type differential mobility analyzers, one for positive and the other for negative ions. The two aspiration condensers are connected as a balanced bridge circuit that allows continuous variation of the driving voltage and scanning of the mobility distribution of charged clusters and nanoparticles, usually called air ions. A large airflow rate 44 liters per second helps to suppress the loss of air ions in the inlet of the instrument. The inlet can be closed or opened for ions using a controlled electrostatic filter and the background signal is eliminated making every second scan with a closed inlet. A mobility distribution is calculated according to the results of 9 scans performed during 3 minutes. The electric mobility range of $0.032\text{--}3.2\text{ cm}^2\text{V}^{-1}\text{s}^{-1}$ is logarithmically uniformly divided into 16 fractions. The mobility distribution is converted to size distribution using the algorithm developed by [Tammet \(1995\)](#). The size distribution is presented by 12 fractions, logarithmically uniformly distributed in the diameter range of 0.4–6.3 nm. The sampling height was about 1.6 m above the ground.

2.2. DMPS

For sub-micron particle sizing the main instrument used was the differential mobility particle sizer (DMPS), operated 2 m above the ground and with a time resolution of 10 min. The system consist of two parallel DMPS devices: one classifying the particles between 3 and 10 nm and the other between 10 and maximum 500 nm. Both devices use a Hauke-type differential mobility analyzer (DMA) ([Winklmayr et al., 1991](#)) and a closed loop sheath flow arrangement ([Jokinen and Mäkelä, 1997](#)). The first device consists of a 10.9 cm long DMA and a TSI model 3025 CPC and the second one of a 28 cm long DMA and a TSI model 3010 CPC. Before sizing the aerosol is neutralized with a 74 MBq (2 mCi) Krypton-85 beta source.

The conventional DMPS measures particle size distributions at dry conditions, RH typically below 10%. In addition to dry conditions, we have measured particle size

Ion production rate

L. Laakso et al.

[Title Page](#)

[Abstract](#)

[Introduction](#)

[Conclusions](#)

[References](#)

[Tables](#)

[Figures](#)

[◀](#)

[▶](#)

[◀](#)

[▶](#)

[Back](#)

[Close](#)

[Full Screen / Esc](#)

[Print Version](#)

[Interactive Discussion](#)

© EGU 2004

distributions at higher relatively humidities with a wet-DMPS system. In the wet-DMPS, aerosol particles are humidified with water vapor before particle size measurement. The wet-DMPS system consists of a Gore-Tex type aerosol humidifier, a Hauke-type DMA (10.9 cm long), a sheath air humidifier unit and an ultrafine CPC (TSI 3025). The construction of the system (e.g. humidifiers) is based on the hygroscopicity tandem DMA described in detail by [Joutsensaari et al. \(2001\)](#). The size distributions were measured every 10 min at RH of 90% for 3–70 nm particles. The sampling height was about 4 m above the ground.

In principle, the freshly formed nucleation mode particles can be observed earlier with the wet-DMPS compared to the dry-DMPS if they grow to detectable size during humidification, i.e. particles below 3 nm in diameter (detection limit of the dry DMPS) at dry conditions can be detected.

2.3. APS

For large-particle sizing, an aerodynamical particle sizer (APS), model TSI 3320, was used. The APS measures particle size distributions from $0.7 \mu\text{m}$ to $20 \mu\text{m}$ by determining the time-of flight of individual particles in an accelerating flow field ([Peters and Leith, 2003](#)). The particle size distributions measured with the APS were shifted to mobility equivalent diameter by dividing the aerodynamic diameter by the square root of the estimated particle density of 1.9 g cm^{-3} . This density was found to give the best consistency between DMPS and APS size distributions ([Aalto et al., 2001](#)) in Hytiälä during previous campaigns.

2.4. Measurements of ionizing radiation

In the lower troposphere, ions are created mainly by cosmic radiation, radiation from the ground and decay of radon emitted from the ground. Both of these ion sources are continuously measured in Hytiälä. The sampling inlet was ca. 6 m above the ground. Measurements of airborne radon-222 have been going on since March 2000.

Ion production rate

L. Laakso et al.

[Title Page](#)

[Abstract](#)

[Introduction](#)

[Conclusions](#)

[References](#)

[Tables](#)

[Figures](#)

[◀](#)

[▶](#)

[◀](#)

[▶](#)

[Back](#)

[Close](#)

[Full Screen / Esc](#)

[Print Version](#)

[Interactive Discussion](#)

© EGU 2004

The ^{222}Rn content of the air was monitored continuously by counting the beta particle emissions of the particle-bound daughter nuclides ^{214}Pb and ^{214}Bi collected onto glass-fibre filters (see Fig. 1). ^{222}Rn , being a noble gas, cannot be collected with aerosol filters. The beta activity of the short-lived ^{222}Rn progeny was distinguished from the ^{220}Rn progeny and artificial radioactivity by their half-life differences (Paatero et al., 1998). The air flow is directed through one of two filters alternately for four-hour periods. The count rate of the Geiger-Mueller (GM) tube increases as beta-active aerosol particles accumulate onto the filter. After four hours the air flow is directed through the other filter. If the beta activity on the first filter is due to ^{222}Rn progeny only, it decays practically completely during the following four hours and the count rate of the GM tube returns to base level. If, however, there is ^{220}Rn progeny or artificial radioactivity present on the filter, the count rate remains above the base line after the four-hour period due to the longer half-lives of these nuclides. ^{222}Rn was assumed to be in equilibrium with its short-lived progeny. The ion pair production rate caused by radon-222 and its short-lived progeny was calculated by taking into consideration the total energy of the three alpha and the two beta particles and by assuming an average energy of 34 eV per produced ion pair.

2.4.2. Measurements of external radiation

External radiation consisting mainly of cosmic radiation and gamma radiation from the ground was measured with a scintillation gamma spectrometer system. A 76 mm \times 76 mm NaI(Tl) detector was placed in a shelter where a constant temperature was maintained. The shelter was located 1.5 m above the ground. The gamma spectra were recorded with a computer add-on board containing a high-voltage supply for the photomultiplier tube, a shaping amplifier and a 1024-channel pulse-height analyzer. The energy spectra between 100 and 3000 keV were acquired in 10-min intervals using a digital spectrum stabilizer. The observed count rates were converted to

Ion production rate

L. Laakso et al.

[Title Page](#)

[Abstract](#)

[Introduction](#)

[Conclusions](#)

[References](#)

[Tables](#)

[Figures](#)

◀

▶

◀

▶

[Back](#)

[Close](#)

[Full Screen / Esc](#)

[Print Version](#)

[Interactive Discussion](#)

© EGU 2004

the dose rate units with a calibration factor obtained by a comparison to a calibrated pressurized ionization chamber. The dose rate values ($\text{mGy h}^{-1} = \text{mJ kg}^{-1} \text{h}^{-1}$) were converted to ion production rate (ion pairs $\text{m}^{-3} \text{s}^{-1}$) by assuming an average energy of 34 eV per produced ion pair.

5 2.5. Ion production rate calculated from ion and aerosol particle measurements

The balance equation for the small cluster ion concentration is (Israel, 1970)

$$\frac{dN_{\pm}}{dt} = Q - \alpha N_{\pm} N_{\mp} - N_{\pm} \int \beta_{\pm}(d_p, q) N(d_p, q), \quad (1)$$

where Q is the ion production rate, N_{\pm} is the concentration of positive or negative cluster ions, α is the ion-ion recombination coefficient, $\beta_{\pm}(d_p, q)$ the cluster ion-aerosol particle attachment coefficient, q is the charge of the aerosol particle and $N(d_p, q)$ the concentration of aerosol particles. The sink of small ions by ion-induced nucleation is not taken into account in this simplified balance equation. In case of charge equilibrium, the derivative in Eq. (2) is equal to zero and thus the ion production rate Q can be obtained. This leads to

$$15 \quad Q = \alpha N_{\pm} N_{\mp} + N_{\pm} \int \beta_{\pm}(d_p, q) N(d_p, q). \quad (2)$$

Because the concentrations of cluster ions and aerosol particles are measured and the recombination and attachment coefficients can be calculated, it is possible to estimate Q from measurements independently of radiation measurements.

Both the DMPS and the APS measured size distributions of dry particles. Thus, the 20 effect of ambient relative humidity had to be somehow taken into account. In this work, we used a simple parameterization suggested by Zhou (2001)

$$GF = (1 - RH/100)^{Y(d_p)}. \quad (3)$$

This parameterization gives the particle growth factor (ie. how much the particle size is increased) due to absorption of water vapour as a function of relative humidity (RH).

Ion production rate

L. Laakso et al.

[Title Page](#)

[Abstract](#)

[Introduction](#)

[Conclusions](#)

[References](#)

[Tables](#)

[Figures](#)

[◀](#)

[▶](#)

[◀](#)

[▶](#)

[Back](#)

[Close](#)

[Full Screen / Esc](#)

[Print Version](#)

[Interactive Discussion](#)

© EGU 2004

The above parameterization was based on the measurements conducted in the Arctic Ocean. Therefore we used $\gamma(dp)$ values obtained by fitting a first order polynomial to the measurements carried out in Hyttiälä during the BIOFOR campaign (Hämeri et al., 2001) for the size range 10–264 nm. The growth factors of possible different externally mixed (hygroscopicity) modes were weighted by their corresponding fractions. The size dependence of the exponential γ was obtained by optimizing a linear function, to obtain

$$\gamma = -3.11 \cdot 10^5 \cdot dp/dp_0 - 0.0847, \quad (4)$$

where the non-dimensionalizing factor dp_0 is 1 m. The growth factors during QUEST 2-campaigns were measured with two independent devices at a constant relative humidity. A Hygroscopic Tandem Differential Mobility analyzer (HTDMA) (see, e.g. Hämeri et al., 2000) measured growth factors for a monodisperse aerosol sample (8, 10, 20 and 50 nm in diameter) at 90% RH. A wet-DMPS was used to measure aerosol growth and the consequent size distribution change at 90% RH for particles from 3 to 70 nm in diameter. The largest contribution to the condensation sink comes from accumulation mode particles, of which we did not have any hygroscopicity measurements. Existing measurements, however, can be used to establish the quality of the parameterization. For 90% RH, the parameterization gives a growth factor of 1.2–1.3. Based on the HTDMA measurements, the average growth factor for 50 nm particles was 1.29 ± 0.11 for the whole campaign period. At the same time the wet-DMPS measurements gave a growth factor of about 1.14 (standard deviation, $\sigma=0.18$) at 90% to the nucleation mode particles (average dry diameter about 20 nm, $\sigma=9$ nm). During nucleation events, an average growth factor and dry particle diameter were about 1.08 ($\sigma=0.14$) and 9 nm ($\sigma=3$ nm), respectively. Thus, the parameterization seems to produce reasonable values in the Aitken size range, whereas it overestimates the growth for the nucleation mode particles.

Based on Eq. (3), the observed dry size spectra were corrected to the ambient relative humidity.

The ion-aerosol attachment coefficients were calculated according to Fuchs attachment theory (Fuchs, 1964) based on measured mobilities and temperatures. The

Ion production rate

L. Laakso et al.

[Title Page](#)

[Abstract](#)

[Introduction](#)

[Conclusions](#)

[References](#)

[Tables](#)

[Figures](#)

[◀](#)

[▶](#)

[◀](#)

[▶](#)

[Back](#)

[Close](#)

[Full Screen / Esc](#)

[Print Version](#)

[Interactive Discussion](#)

masses of the ions were estimated according to the method given by Tammet (1998), in which the small ion mass is correlated with its mobility by

$$K = \left(\frac{1200 u}{m_{\text{ion}}} \right)^{1/3} - 0.2 \quad (5)$$

where K is in $\text{cm}^2 \text{V}^{-1} \text{s}^{-1}$, and the mass is in the range of 30–2100 u. The correlation is based on experimental data by Kilpatrick (1971). Next the mean mobility of cluster ions was calculated based on BSMA-measurements. Only negative ions were utilized in our studies since positive ions gave approximately similar results. Finally, Eq. (2) was solved for each individual measured particle size distribution spectrum to obtain the ion production rate Q .

10 3. Results

In this study, we used the period 20 March–11 April 2003 or days 79–101 of the year. All data was interpolated to correspond to the time resolution of the BSMA, namely 360 s. The average ion production rate calculated from DMPS, APS and BSMA-measurements were $2.6 \text{ cm}^{-3} \text{ s}^{-1}$ and from external radiation and radon measurements $15 4.5 \text{ cm}^{-3} \text{ s}^{-1}$ (Table 1). During the study period the amount of ^{220}Rn progeny and artificial radioactivity in the air was insignificant compared to the amount of ^{222}Rn .

In case of direct measurements the external radiation is mostly responsible for the ion production, the contribution of radon is about 10% in general, a maximum of 36% was recorded on 26 March 1999 in Hyytiälä. In case of model calculations (Eq. 2) the ion production rate is mainly influenced by the concentration of particles in the size range of 5–500 nm measured by means of DMPS, the contribution of large particles (measured by APS) is always less than 10%, having an average about 2%. Also the effect of ion-ion recombination is significant.

An example of the size distribution of the ion sink caused by aerosol particles, the term $dN/d\log(d_p) \cdot \beta_{\pm}(d_p, q)$ is shown in Fig. 2. This figure is drawn using the aver-

Ion production rate

L. Laakso et al.

[Title Page](#)

[Abstract](#)

[Introduction](#)

[Conclusions](#)

[References](#)

[Tables](#)

[Figures](#)

[◀](#)

[▶](#)

[◀](#)

[▶](#)

[Back](#)

[Close](#)

[Full Screen / Esc](#)

[Print Version](#)

[Interactive Discussion](#)

age mobility $1.23 \cdot 10^{-4} \text{ cm}^2 \text{V}^{-1} \text{s}^{-1}$, temperature $+5^\circ\text{C}$ and relative humidity 90%. Size ranges of DMPS and APS corresponding to relative humidity 90% are also shown. From this figure it can be seen that the ion sink is dominated by particle diameter range 30–700 nm.

5 In Fig. 3 the ion production rates calculated with the two different methods are shown. The overall behavior show similar behavior in both measurements, the highest ion production rates being in the middle of the period. The ion production rates obtained from external radiation and radon measurements have much less variability than the rates calculated from ion and particle measurements. One similar feature for both methods
10 is that the ion production rate is highest during nighttime. This is assumed to be due to radon accumulation on the surface layer during the stable nighttime conditions. One good measure of boundary layer stability is the so-called Flux Richardson number Rf (Seinfeld and Pandis, 1998) which is based on heat and momentum fluxes measured by eddy covariance technique. In Fig. 4 Rf is shown together with the radon-based ion
15 production rate. During the night Rf is often positive representing stable conditions. The curves representing Rf and radon-based ion production have certain features: the ion production rate is peaking after Rf because radon is accumulating during the night and the concentration reaches its maximum in the early morning. During day 81 there
20 is only very little mixing, so radon is accumulating for a longer period than one night.

25 To check the effect of the growth factor parameterization to the results, the growth factors were varied by $\pm 10\%$. The resulting ion production rates were $2.4 \text{ cm}^{-3} \text{ s}^{-1}$ and $2.9 \text{ cm}^{-3} \text{ s}^{-1}$, so the hygroscopic growth factor has indeed a significant effect on the ion sink and therefore on the calculated ion production rate in this case. In addition the diurnal cycle of RH amplifies the effect. However, it can not explain the systematic differences between the ion production rates obtained by these two methods. Two other tests were made to check the assumptions used in calculations. One average cluster ion size instead of six cluster ion size intervals were used in the calculations. The effect of this approximation was on the average less than one percent compared to the case where the ion loss rate was calculated separately for all these six size classes

Ion production rate

L. Laakso et al.

[Title Page](#)

[Abstract](#)

[Introduction](#)

[Conclusions](#)

[References](#)

[Tables](#)

[Figures](#)

[◀](#)

[▶](#)

[◀](#)

[▶](#)

[Back](#)

[Close](#)

[Full Screen / Esc](#)

[Print Version](#)

[Interactive Discussion](#)

© EGU 2004

and then summed up.

Another approximation was made regarding hygroscopic growth. We used one average growth factor for all particles of a certain size. However, in reality, there is normally several external hygroscopic growth modes present in the atmosphere (Hämeri et al., 2001). Because the ion loss is proportional to the diameter of the particle, using an average growth factor may lead to erroneous results. The effect of hygroscopic mode separation was found to be less than 5% compared to one average growth factor.

In case of high relative humidity, there may be fog formation causing an additional sink to the ions. Unfortunately, we did not have fog measurements during the QUEST 10 2-campaign. However, at least during days 81, 89 and 95 the relative humidity stayed high all day (Fig. 5) which indicates fog formation and thus an increased ion loss rate. The same applies for rain episodes: it is observed that rain droplets are charged, consequently the scavenging of ions onto rain droplets may reduce the concentration of ions. However, there was practically no rain during the period; only during days 89 and 15 95 there was some precipitation. Based on earlier data from the BIOFOR III-campaign (Hörrak et al., 2003), it seems that rain does not normally change the concentration of small ions significantly. There were clearly lower concentrations only when the RH was more than 98%. During the whole period used in present study, there was snow cover in Hyytiälä measurement station.

20 During the nucleation bursts, there is a possible additional sink of small ions by ion-induced nucleation. It is observed, that the nanometer particles are sometimes slightly overcharged (Laakso et al., 2004), which indicates the effect of ions on nucleation process, at least in a certain degree. Another, more probable ion sink during the nucleation burst is caused by the particles in the diameter range of 1.5–3 nm, which is not measured by common aerosol instruments. If we for example assume the concentration of 25 1.5–3 nm particles to be about $30\,000\text{ cm}^{-3}$, a value based on model studies (Laakso et al., 2004), and that of small ions about 1000 cm^{-3} , the value for additional ion sink is of the order $1\text{ cm}^{-3}\text{s}^{-1}$ during the nucleation bursts.

Particle concentration below the detection limit of the dry DMPS (3 nm) can be es-

Ion production rate

L. Laakso et al.

[Title Page](#)

[Abstract](#)

[Introduction](#)

[Conclusions](#)

[References](#)

[Tables](#)

[Figures](#)

[◀](#)

[▶](#)

[◀](#)

[▶](#)

[Back](#)

[Close](#)

[Full Screen / Esc](#)

[Print Version](#)

[Interactive Discussion](#)

© EGU 2004

timated from wet-DMPS results since the particles can grow to detectable size during humidification. A rough estimation of concentration of 2.5–3.0 nm particles has been calculated assuming that the growth factor of the fine particles is about 1.2. The average concentration is about 200 cm^{-3} over all measurement days and about 700 cm^{-3} during nucleation events. The maximum observed 2.5–3 nm particle concentration is around 8000 cm^{-3} which indeed has a significant effect on ion concentration during the nucleation events.

One of the most interesting features of these kind of calculations is that they offer us a method to study existence of so called thermodynamically stable clusters (TSCs) (Kulmala et al., 2000b). TSCs cannot be observed directly by standard aerosol size distribution measurements because of their small size (of order 1 nm). If the background particle concentration is so high that it hinders the particle growth to observable sizes, there can still be enough particles to cause an additional ion sink which can be seen from the difference of calculated and radon and external radiation based measurements. It has been previously found that TSC's can form nearly every day, but they can only be observed if they can grow to sufficiently large sizes before they are scavenged. If we now for example compare sunny (= there is sulphuric acid formation) and cloudy days with relative high background concentrations, we may see a difference caused by the TSC's. This possibility is however mixed with the possibility of the contribution of ion-induced ion-accelerated cluster formation (Laakso et al., 2004).

There are some causes of uncertainties in our analysis. The orography of the measurement locations may have a small effect on the systematic differences between these two methods, this because the concentrations of radon and ions were measured few tens of meters apart and at heights of about 6 and 2 m, respectively. The forest canopy may also provide an additional sink for the ions, which was not taken into account in this study. The applied model of the ionization process has also some degree of approximation. The measured dose rate and radon concentration data was converted to ion production rate by assuming that all the energy goes to ionization and that it takes 34 eV to produce one ion pair in air. In reality a part of the energy is,

Ion production rate

L. Laakso et al.

[Title Page](#)

[Abstract](#)

[Introduction](#)

[Conclusions](#)

[References](#)

[Tables](#)

[Figures](#)

[◀](#)

[▶](#)

[◀](#)

[▶](#)

[Back](#)

[Close](#)

[Full Screen / Esc](#)

[Print Version](#)

[Interactive Discussion](#)

© EGU 2004

however, consumed to other processes. After the alpha particle emission the recoiling daughter nucleus can also cause intense ionization but within a very short distance.

The most major uncertainty is probably related to the lack of knowledge on the ion-ion recombination process in the real atmosphere. The recombination is three-body process (Bates, 1985), and depends on the mobility and energy of ions. The mobility depends on ion-cluster formation (initial species, free electron and positively charged kernel of “air molecule” after about 1 microsecond form ion clusters). It is rational to assume that the recombination rate of ion-clusters just after the ionization act in the vicinity of “ionization-track” is higher than after its dispersion. Therefore the recombination rate is dependent on the type of ionizing radiation (alpha, beta, gamma); it is the highest in the case of alpha-radiation (short tracks) and the lowest in the case of gamma-radiation (uniform ionization through the volume). In this study we used the value $1.6 \cdot 10^{-6} \text{ cm}^3 \text{s}^{-1}$ for the recombination coefficient, a value often cited in the textbooks of atmospheric electricity (Israel, 1970).

In addition to studied period, one particular day 25 March 2003 (day 84) was chosen to be investigated in more detail. This day was chosen because it was one of the best particle formation days during the campaign. The number distribution evolution as well as the total number concentration evolution of the day are shown in Fig. 6. During this day the ion production rates estimated by the two methods displayed nearly equal values during nighttime, but showing considerable difference during daytime.

The contributions of different model calculations and radiation measurements on 25 March 2003 are shown In Fig. 7 and Table 1. Recombination is quite steady during the day, whereas some other sinks are underestimated. The expected increment of the ion production rate of about $1 \text{ cm}^{-3} \text{s}^{-1}$ caused by an additional hypothetical sink of small ions, followed the generation of 1.5–3 nm particles of about $30\,000 \text{ cm}^{-3}$ around noon, is enough to explain the discrepancy between the results of two methods in this case.

[Title Page](#)[Abstract](#)[Introduction](#)[Conclusions](#)[References](#)[Tables](#)[Figures](#)[◀](#)[▶](#)[◀](#)[▶](#)[Back](#)[Close](#)[Full Screen / Esc](#)[Print Version](#)[Interactive Discussion](#)

4. Conclusions

ACPD

4, 3947–3973, 2004

In this study the ion production rates in a boreal forest were studied based on two different methods: 1) external radiation and radon concentration, 2) ion and particle concentrations. Both methods produced reasonable estimates for the ion production rates. The average ion production rate calculated from DMPS, APS and BSMA-measurements was $2.6 \text{ cm}^{-3} \text{ s}^{-1}$ and based on external radiation and radon measurements $4.5 \text{ cm}^{-3} \text{ s}^{-1}$. The first method based on ion and particle measurements underestimates the ion production rates especially during the day. There are two main reasons for this underestimation: the particle measurements start only from 3 nm, so the sink of ions during the nucleation events is underestimated. Another reason is the possible fogs during the day. One more possible reason for the discrepancy is the nucleation mechanism itself, if the ions are somehow present in the nucleation process, there may be an additional ion sink during the nucleation days. On the other hand, not all the radiation energy is converted to ions and the possible effect of alpha recoil is also omitted.

Acknowledgements. P. P. Aalto is acknowledged for his significant contribution to the measurements.

References

Aalto, P., Hämeri, K., Becker, E., Weber, R., Salm, J., Mäkelä, J. M., Hoell, C., O'Dowd, C. D., Karlsson, H., Hansson, H.-C., Väkevä, M., Koponen, I. K., Buzorius, G., and Kulmala, M.: Physical characterization of aerosol particles during nucleation events, Tellus, 53B, 344–358, 2001. [3953](#)

Bates, D.: Ion-ion recombination in an ambient gas, Adv. At. Mol. Phys., 20, 1–40, 1985. [3961](#)

Chalmers, J.: Atmospheric Electricity, Pergamon Press, Oxford, London, 1967. [3949](#)

Dhanorkar, S. and Kamra, A.: Diurnal variation of ionization rate close to ground, J. Geophys. Res., 99, 18 523–18 526, 1994. [3950](#)

Dolazalek, H.: The atmospheric electric fog effect, Rev. Geophys., 1, 231–282, 1963. [3951](#)

Ion production rate

L. Laakso et al.

[Title Page](#)

[Abstract](#)

[Introduction](#)

[Conclusions](#)

[References](#)

[Tables](#)

[Figures](#)

[◀](#)

[▶](#)

[◀](#)

[▶](#)

[Back](#)

[Close](#)

[Full Screen / Esc](#)

[Print Version](#)

[Interactive Discussion](#)

© EGU 2004

Fuchs, N. A.: The mechanics of Aerosol, Pergamon, New York, 1964. [3956](#)

Hörrak, U., Aalto, P., Salm, J., and Kulmala, M.: Characterization of air ions during nucleation events in boreal forest air, in Report Series in Aerosol Science 59, 196–201, 2003. [3959](#)

Hämeri, K., Väkevä, M., Hansson, H.-C., and Laaksonen, A.: Hygroscopic growth of ultrafine ammonium sulphate aerosol measured using an ultrafine tandem differential mobility analyser, *J. Geophys. Res.*, 105, 22231–22242, 2000. [3956](#)

Hämeri, K., Väkevä, M., Aalto, P. P., Kulmala, M., Swietlicki, E., Zhou, J., Seidl, W., Becker, E., and O'Dowd, C. D.: Hygroscopic and CCN properties of aerosol particles in boreal forests, *Tellus*, 53B, 359–379, 2001. [3956](#), [3959](#)

Hensen, A. and van der Hage, J. C. H.: Parametrization of cosmic radiation at sea level, *J. Geophys. Res.*, 99, 10 693–10 695, 1994. [3950](#), [3951](#)

Hoppel, W., Anderson, R., and Willett, J.: The Earths Electrical Environment, chap. Atmospheric electric, National Academy Press, Washington, D.C., 149–165, 1986. [3949](#), [3951](#)

Israel, H.: Atmospheric electricity, Israel Program for Scientific Translations, Jerusalem, Vol 1., 1970. [3949](#), [3955](#), [3961](#)

Israel, H.: Atmospheric electricity, Israel Program for Scientific Translations, Jerusalem, Vol. 2, 1973. [3949](#)

Jokinen, V. and Mäkelä, J. M.: Closed loop arrangement with critical orifice for DMA sheath/excess flow system, *J. Aerosol Sci.*, 28, 643–648, 1997. [3952](#)

Joutsensaari, J., Vaattovaara, P., Hämeri, K., and Laaksonen, A.: A novel tandem differential mobility analyser with organic vapor treatment of aerosol particles, *Atmos. Chem. Phys. Discuss.*, 1, 1–22, 2001. [3953](#)

Kataoka, T., Yunoki, E., Shimizu, M., Mori, T., Tsukamoto, O., Ohhashi, Y., Sahashi, K., Maitani, T., Miyashita, K., Fujikawa, Y., and Kudo, A.: Diurnal variation in radon concentration and mixing-layer depths, *Boundary-Layer Meteorology*, 89, 225–250, 1998. [3950](#)

Kilpatrick, W.: An experimental mass-mobility relation for ions in air at atmospheric pressure, in *Proc. Annu. Conf. Mass. Spectrosc.* 19th., 320–325, 1971. [3957](#)

Kulmala, M., Korhonen, P., Laakso, L., and Pirjola, L.: Nucleation in boreal forest boundary layer, *Environ. Chem. Physics*, 22, 46–53, 2000a. [3948](#)

Kulmala, M., Pirjola, L., and Mäkelä, J. M.: Stable sulphate clusters as a source of new atmospheric particles, *Nature*, 404, 66–69, 2000b. [3960](#)

Kulmala, M., Hämeri, K., Aalto, P., Mäkelä, J., Pirjola, L., Nilsson, E. D., Buzorius, G., Rannik, Ü., Dal Maso, M., Seidl, W., Hoffmann, T., Jansson, R., Hansson, H.-C., O'Dowd, C., and

Ion production rate

L. Laakso et al.

Title Page

Abstract

Introduction

Conclusions

References

Tables

Figures

◀

▶

◀

▶

Back

Close

Full Screen / Esc

Print Version

Interactive Discussion

© EGU 2004

Viisanen, Y.: Overview of the international project on biogenic aerosol formation in the boreal forest (BIOFOR), *Tellus B*, 53, 324–343, 2001. [3951](#)

Kulmala, M., Vehkamäki, H., Petäjä, T., Dal Maso, M., Lauri, A., Kerminen, V.-M., Birmili, W., and McMurry, P.: Formation and growth rates of ultrafine atmospheric particles: a review of observations, *J. Aerosol Sci.*, 35, 143–176, 2004. [3948](#)

5 Laakso, L., Anttila, T., Lehtinen, K. E. J., Aalto, P. P., Kulmala, M., Hõrrak, U., Paatero, J., Hanke, M., and Arnold, F.: Kinetic nucleation and ions in boreal particle formation events, *Atmos. Chem. Phys. Discuss.*, accepted, 2004. [3948](#), [3959](#), [3960](#)

Larsen, R.: Global decrease of beryllium-7 in surface air, *Journal of Environmental Radioactivity*, 18, 85–87, 1993. [3950](#)

10 Liu, S., McAfee, J., and Cicerone, R.: Radon-222 and Tropospheric Vertical Transport, *J. Geophys. Res.*, 89, 7291–7297, 1984. [3950](#)

Mochizuki, S., Namiki, Y., Kato, T., Masuda, S., and Sekikawa, T.: Electrical Processes in Atmospheres, chap. A technique for cont, Dr. Dietrich Steinkopff Verlag, Darmstadt, Germany, 15 204–210, 1977. [3950](#)

Mohnen, V.: Electrical Processes in Atmospheres, chap. Formation, nature an, Dr. Dietrich Steinkopff Verlag, Darmstadt, Germany, 1–17, 1977. [3949](#)

Paatero, J., Hatakka, J., and Viisanen, Y.: Concurrent Measurements of Airborne Radon-222, Lead-210 and Beryllium-7 at the Pallas-Sodankylä GAW Station, Northern Finland, Tech. 20 rep., Finnish Meteorological Institute, 1998. [3954](#)

Peters, T. M. and Leith, D.: Concentration measurement and counting efficiency of the aerodynamic particle sizer 3321, *J. Aerosol Sci.*, 34, 627–634, 2003. [3953](#)

Porstendorfer, J.: Properties and behaviour of radon and thoron and their decay products in the air, *J. Aerosol Sci.*, 25, 219–263, 1994. [3950](#)

25 Rosen, J., Hofmann, D., and Gringel, W.: Measurements of ion mobility to 30 km, *J. Geophys. Res.*, 90, 5876–5884, 1985. [3949](#)

Seinfeld, J. H. and Pandis, S. N.: Atmospheric Chemistry and Physics: From Air Pollution to Climate Change, Wiley, New York, 1998. [3958](#)

Tammet, H.: Size and mobility of nanometer particles, clusters and ions, *J. Aerosol Sci.*, 26, 30 459–475, 1995. [3952](#)

Tammet, H.: Reduction of air ion mobility to standard conditions, *J. Geophys. Res.-A*, 103, 13 933–13 937, 1998. [3957](#)

Vesala, T., Haataja, J., Aalto, P., Altimir, N., Buzorius, G., Garam, E., Hämeri, K., Ilvesniemi, H.,

Jokinen, V., Keronen, P., Lahti, T., Markkanen, T., Mäkelä, J., Nikinmaa, E., Palmroth, S., and Palva, L.: Long-term field measurements of atmosphere-surface interactions in boreal forest combining forest ecology, micrometeorology, aerosol physics and atmospheric chemistry, *Trends in Heat, Mass & Momentum Transfer*, 4, 17–35, 1998. [3951](#)

5 Wilkening, M.: Characteristics of atmospheric ions in contrasting environments, *J. Geophys. Res.*, 90, 5933–5935, 1985. [3950](#)

Winklmayr, W., Reischl, G., Lindner, A., and Berner, A.: A new electromobility spectrometer for the measurement of aerosol size distributions in the size range from 1 to 1000 nm, *J. Aerosol Sci.*, 22, 289–296, 1991. [3952](#)

10 Yu, F. and Turco, R. P.: Ultrafine aerosol formation via ion-mediated nucleation, *Geophys. Res. Lett.*, 27, 883–886, 2000. [3948](#), [3949](#)

Zhou, J.: Hygroscopic properties of atmospheric aerosol particles in various environments, Ph.D. thesis, University of Lund, Division of Nuclear Physics, Sweden, 2001. [3955](#)

Ion production rate

L. Laakso et al.

[Title Page](#)

[Abstract](#)

[Introduction](#)

[Conclusions](#)

[References](#)

[Tables](#)

[Figures](#)

[◀](#)

[▶](#)

[◀](#)

[▶](#)

[Back](#)

[Close](#)

[Full Screen / Esc](#)

[Print Version](#)

[Interactive Discussion](#)

© EGU 2004

Ion production rate

L. Laakso et al.

Table 1. Statistical characteristics (mean, 25%, 50%, 75% quantiles and standard deviation) of estimated ion production rates, in $\text{cm}^{-3}\text{s}^{-1}$.

		Whole period					Day 84 (25 March)				
		Mean	25%	50%	75%	σ	Mean	25%	50%	75%	σ
Measured	External	3.99	3.51	3.68	4.60	0.59	3.93	3.90	3.92	3.95	0.03
	Radon	0.34	0.23	0.43	0.65	0.32	0.35	0.13	0.27	0.58	0.22
	Sum	4.47	3.74	4.11	5.25	–	4.27	4.03	4.19	4.53	–
Calculated	DMPS-range	1.93	1.28	2.02	2.92	0.93	1.74	1.17	1.67	2.23	0.71
	APS-range	0.09	0.03	0.05	0.13	0.30	0.06	0.02	0.03	0.09	0.05
	Recombination	0.64	0.42	0.69	1.04	0.39	0.99	0.76	0.89	1.15	0.34
	Sum	2.63	2.08	2.74	3.96	–	2.79	1.94	2.86	3.47	–

Title Page

Abstract

Introduction

Conclusions

References

Tables

Figures

◀

▶

◀

▶

Back

Close

Full Screen / Esc

Print Version

Interactive Discussion

© EGU 2004

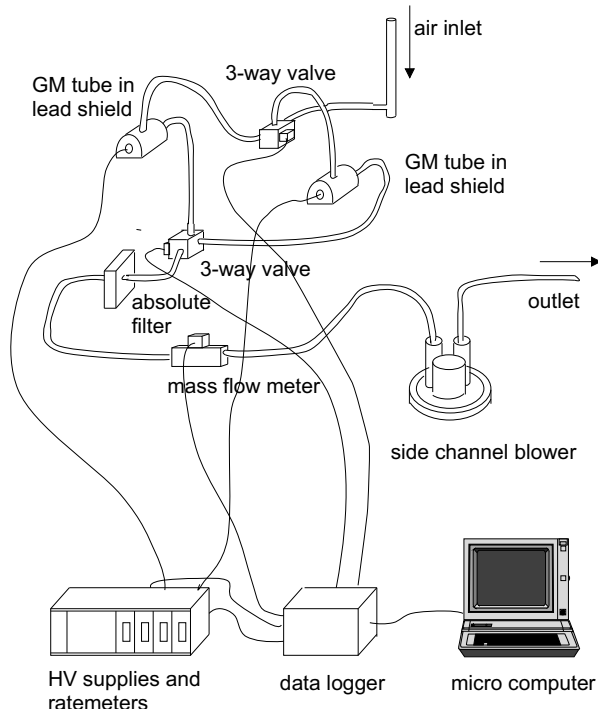


Fig. 1. Setup of the radon monitoring system (HV: high voltage, GM: Geiger-Mueller).

Ion production rate

L. Laakso et al.

[Title Page](#)

[Abstract](#)

[Introduction](#)

[Conclusions](#)

[References](#)

[Tables](#)

[Figures](#)

[◀](#)

[▶](#)

[◀](#)

[▶](#)

[Back](#)

[Close](#)

[Full Screen / Esc](#)

[Print Version](#)

[Interactive Discussion](#)

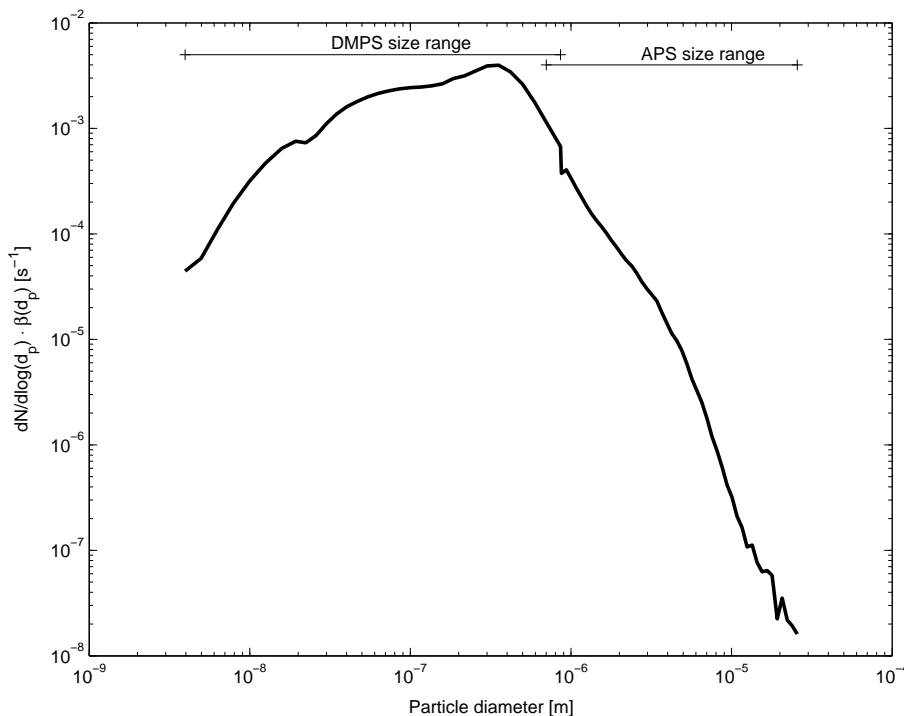


Fig. 2. Average factor $dN/d\log(d_p) \cdot \beta(d_p, q)$ (see Eq. 2) for period from 20 March to 13 April 2003. Size ranges of DMPS and APS corresponding to relative humidity 90% are also shown.

Ion production rate

L. Laakso et al.

[Title Page](#)

[Abstract](#)

[Introduction](#)

[Conclusions](#)

[References](#)

[Tables](#)

[Figures](#)

◀

▶

◀

▶

[Back](#)

[Close](#)

[Full Screen / Esc](#)

[Print Version](#)

[Interactive Discussion](#)

© EGU 2004

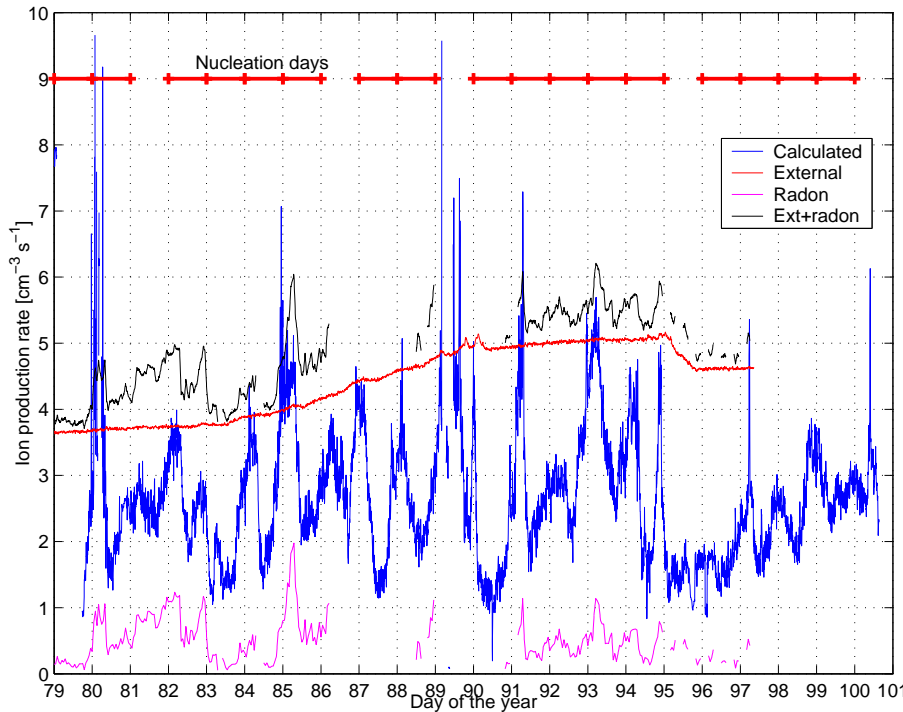


Fig. 3. Ion production rates calculated from external radiation and radon measurements and based on DMPS, BSMA and APS measurements. In addition, days with clear particle formation are shown.

Ion production rate

L. Laakso et al.

[Title Page](#)

[Abstract](#)

[Introduction](#)

[Conclusions](#)

[References](#)

[Tables](#)

[Figures](#)

[◀](#)

[▶](#)

[◀](#)

[▶](#)

[Back](#)

[Close](#)

[Full Screen / Esc](#)

[Print Version](#)

[Interactive Discussion](#)

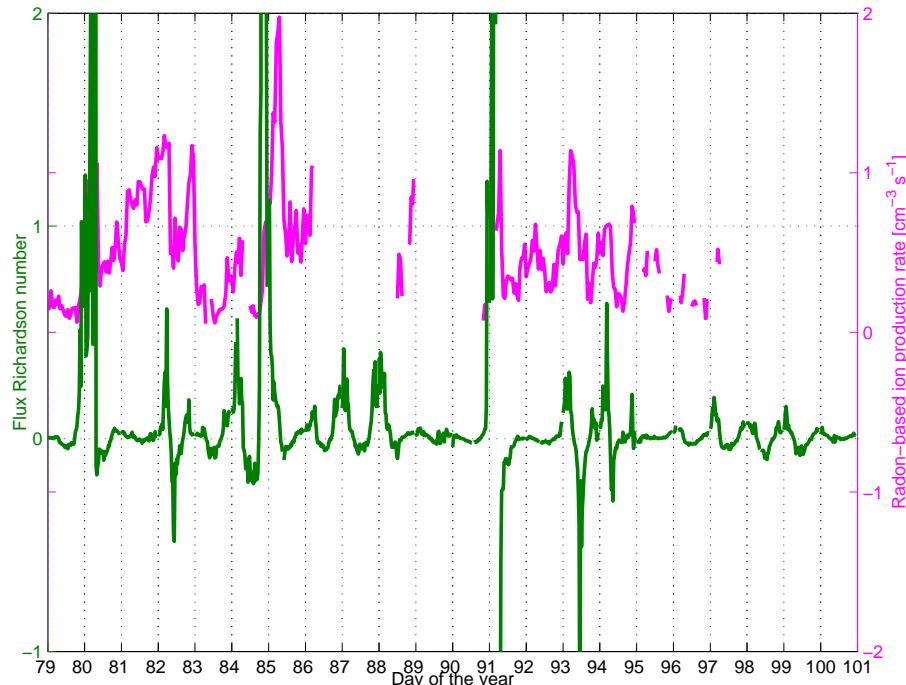


Fig. 4. Radon-based ion production and the stability of the lower boundary layer indicated by the flux Richardson number Rf .

Ion production rate

L. Laakso et al.

[Title Page](#)

[Abstract](#)

[Introduction](#)

[Conclusions](#)

[References](#)

[Tables](#)

[Figures](#)

[◀](#)

[▶](#)

[◀](#)

[▶](#)

[Back](#)

[Close](#)

[Full Screen / Esc](#)

[Print Version](#)

[Interactive Discussion](#)

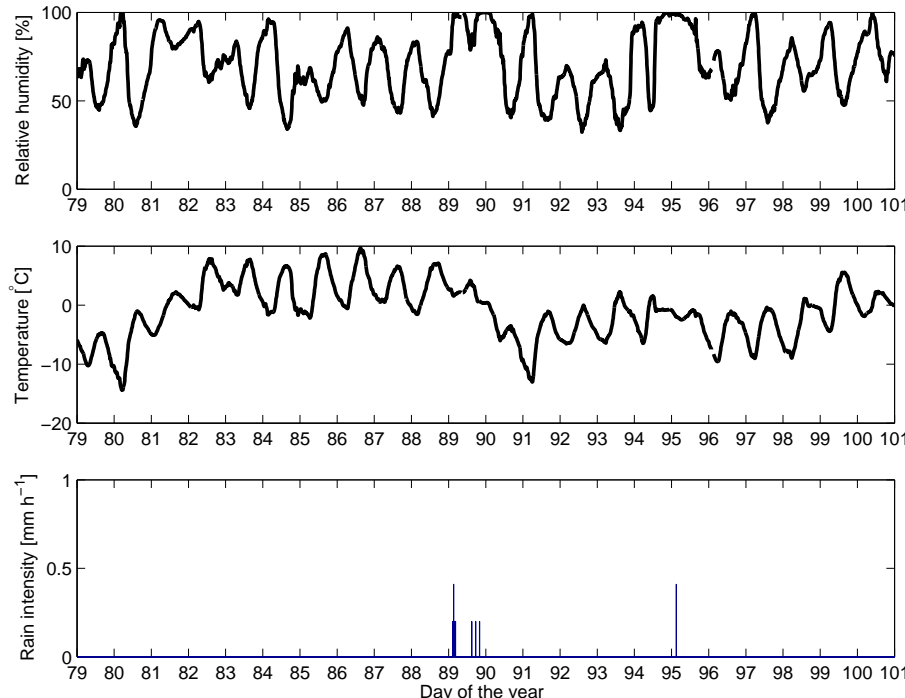


Fig. 5. Relative humidity, air temperature and rain intensity during the QUEST 2-campaign.

Ion production rate

L. Laakso et al.

[Title Page](#)

[Abstract](#)

[Introduction](#)

[Conclusions](#)

[References](#)

[Tables](#)

[Figures](#)

[◀](#)

[▶](#)

[◀](#)

[▶](#)

[Back](#)

[Close](#)

[Full Screen / Esc](#)

[Print Version](#)

[Interactive Discussion](#)

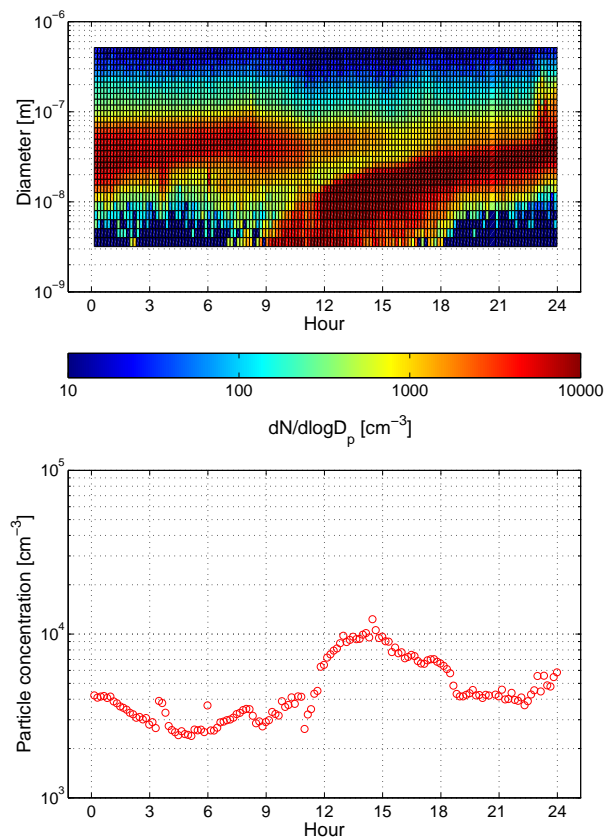


Fig. 6. Particle size spectrum measured by DMPS in 25 March 2003 (upper panel) and the particle concentrations with diameter from 3 to 500 nm as a function of time of the day (lower panel).

Ion production rate

L. Laakso et al.

[Title Page](#)

[Abstract](#)

[Introduction](#)

[Conclusions](#)

[References](#)

[Tables](#)

[Figures](#)

[◀](#)

[▶](#)

[◀](#)

[▶](#)

[Back](#)

[Close](#)

[Full Screen / Esc](#)

[Print Version](#)

[Interactive Discussion](#)

© EGU 2004

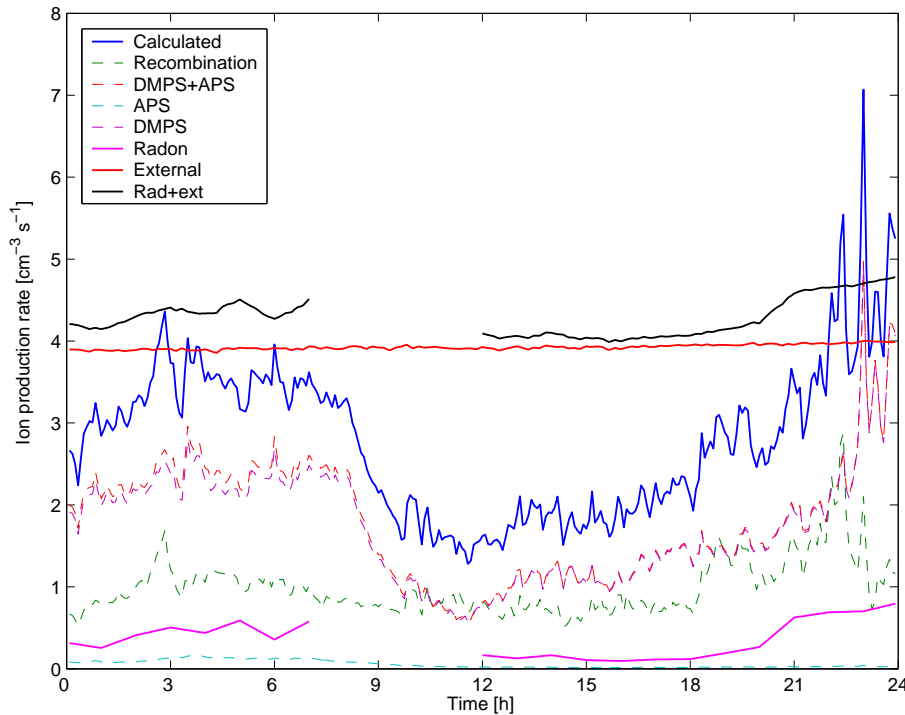


Fig. 7. Ion production rate during on 25 March 2003 (day 84). Calculated mean of the sum of recombination and APS- and DMPS-size ranges, All particles is the combination of DMPS- and APS-size ranges.

Ion production rate

L. Laakso et al.

[Title Page](#)

[Abstract](#)

[Introduction](#)

[Conclusions](#)

[References](#)

[Tables](#)

[Figures](#)

◀

▶

◀

▶

[Back](#)

[Close](#)

[Full Screen / Esc](#)

[Print Version](#)

[Interactive Discussion](#)

© EGU 2004